A Robust Approach for Repairing Color Composite DMC Images

Jun Pan, Mi Wang, Deren Li, and Jonathan Li

Abstract

The aerial images acquired by Intergraph's Digital Mapping Camera (DMC) have been normally used for generating photogrammetric products such as Digital Terrain Models (DTM) and orthophotos. Our experience shows that the failure of radiometric correction in postprocessing leads to residual radiometric differences between CCD images, which then affect the quality of the images for further applications. This paper presents a robust approach to repair defects due to the residual radiometric differences. The approach comprises the auto-locating for the transition area and seamline, and the subsequent reconstruction for image in radiometry. A hierarchical strategy for auto-locating is employed to reinforce the robustness, and a multi-scale strategy is adopted to optimize the adjustment in order to reduce the effect of the change of features in image during the subsequent reconstruction in radiometry. Experiments are designed for the validation of the proposed algorithm, in which both qualitative and quantitative analyses are applied to evaluate the performance of the algorithm. The algorithm has been embedded into GeoDodging 4.0 software package (Wuda Geoinformatics Co., Ltd., China), which is specialized in image dodging and mosaicking, as a complementary module for the postprocessing of DMC images.

Introduction

Digital aerial cameras have many advantages compared with the film-based cameras: the inherent geometric stability (flatness of the image plane and no film shrinkage), the high radiometric image quality, the quick availability of the image data, and no need for a film processing lab (Tang *et al.*, 2000; Madani *et al.*, 2004). Therefore, airborne digital cameras based on different technical concepts have been increasingly used for photogrammetric mapping.

Ideally, a single chip with appropriate size and resolution should be used to transfer the photogrammetric capabilities of film-based cameras (e.g., RMK-TOP) to that of their digital counterparts. However, such a chip with such a large-format is not yet available for technological and economic reasons. Since a large field-of-view is mandatory in photogrammetric mapping due to the high accuracy requirement and economic considerations, several Charge-Coupled Device (CCD) sensors are combined to deliver the large ground coverage (Dörstel and Zeitler, 2002).

Various digital aerial cameras have been developed by a combination of several camera modules on matrix-based CCD sensors to achieve high geometrical resolution and accuracy together with large ground coverage such as UltraCam_X/UltraCam_D (Vexcel, 2008), DIMAC (DiMAC Systems, 2007), including the Intergraph Digital Mapping Camera (DMC). DMC is a digital aerial camera consisting of eight internal sensors: four panchromatic (PAN) sensors and four multispectral sensors. The multispectral sensors are 3,000 pixels by 2,000 pixels each in dimension and capture red, green, blue, and near-infrared data, respectively. The four PAN sensors each capture one image of a defined area (7,000 pixels by 4,000 pixels each), which slightly overlap with one another and are used to produce one large mosaic image with dimensions of 7,680 pixels by 13,824 pixels. The multispectral image has the same ground coverage as the virtual large-format PAN image but only about one-sixteenth part of the number of pixels (Diener *et al.*, 2000; Dörstel and Zeitler, 2002; Madani *et al.*, 2004). During postprocessing, the radiometric and geometric correction is first performed for each DMC image with the camera calibration data. Then, the four PAN images are mosaicked and geometrically converted to a virtual image, which has a new virtual camera constant and can be considered as an ideal photogrammetric image. Parallel to image conversion, the individual multispectral channels are combined. Red, green, and blue (RGB) channels are first combined to produce a natural color image, while the near-infrared (NIR) channel is used to produce a false color image. Then, a color image is combined together with the virtual image by image fusion to form a color composite DMC image (Hinz *et al.*, 2000; Heier *et al.*, 2002).

The DMC has been widely used for photogrammetric mapping in China, and our experience shows that the failure of radiometric correction in postprocessing leads to residual radiometric differences in the final color composite DMC images, which affects the quality of the images to be used for further applications. Because the color composite DMC images are the fusion and mosaic of several small CCD images and there is no visible seam, existing stitching algorithms (e.g., Milgram, 1975; Burt and Adelson, 1983; Afek and Brand, 1998; Zomet *et al.*, 2006) may not achieve satisfactory results. To this end, Wang *et al.* (2005) presented

Jun Pan, Mi Wang, and Deren Li are with the State Key Laboratory of Information Engineering in Surveying, Mapping and Remote Sensing, Wuhan University, 129 Luo Yu Road, Wuhan, Hubei, China 430079 (wangmi@x263.net).

Jonathan Li is with the Department of Geography, Faculty of Environmental Studies, University of Waterloo, 200 University Avenue West, Waterloo, Ontario, Canada N2L 3G1, and a Guest Professor with the State Key Laboratory of Information Engineering in Surveying, Mapping and Remote Sensing, Wuhan University.

Photogrammetric Engineering & Remote Sensing
Vol. 75, No. 2, February 2009, pp. 201–210.

0099-1112/09/7502–0201/$3.00/0

an approach to remove the residual radiometric differences, but it could not locate the transition area and seamlines automatically. Pan *et al.* (2006) studied this fea-sibility, but their approach was not robust and did not take into account all factors. Therefore, we present a robust approach in this paper to repair the images with residual radiometric differences.

This paper is organized as follows. After the principle is described, the proof about the feasibility to locate the transition area and seamline is given. Then, the proposed algorithm is described in detail followed by demonstrating experimental results with discussions and conclusions.

Description of Proposed Algorithm

Color composite DMC images are the fusion and mosaic of several small CCD images together in postprocessing. Figure 1 illustrates the mosaicking procedure, in which Figure 1a shows the geometric aspect (Tang *et al.*, 2000; Madani *et al.*, 2004). The dashed rectangle area denotes the scope of the color composite DMC image and the shaded area in the middle are the tie point area. As far as the radiometric aspect is concerned, it is assumed that the mosaicking procedure can be considered as what is shown in Figure 1b based on analyzing the color composite DMC images. Each rectangle between two adjacent CCD images is the transition area, and the dashed line in each transition area is the seamline. Thus, there are a total of four transition areas and four seamlines for each image. During mosaicking, the left image values are taken in the left area of the seamline, while the right image values are taken in the right area, and a smooth transition in radiometry is achieved in the transition area.

The section map across the transition area for color composite DMC images with three possible cases is illustrated in Figure 2. Figure 2a and 2b show the two cases with residual radiometric differences, while 2c shows the case without radiometric differences. The curve denotes the distribution of pixel values across the transition area between points A and B, point O is the position of the seamline, and Δg denotes the radiometric differences between CCD images around the transition area.

Residual radiometric differences in color composite DMC images are completedy caused by the formation of the large format PAN virtual image which negatively affects the later image fusion process. There are no errors in the color channels, and the fusion of high-resolution PAN image and low-resolution RGB image results in errors. During the formation of the large format PAN virtual image, if not being calibrated effectively, residual radiometric differences after mosaicking remain, and various reasons for the radiometric differences among four PAN CCD images exist. The factors leading to the radiometric differences may include:

1. Defective pixels, including individual pixels with poor electronic quality or missing individual pixels.
2. Different light sensitivities of each single pixel of a CCD.
3. Effect of lenses and aperture.
4. Effect of the time delayed integration (TDI).
5. Effect of the dark current on the resulting values of CCD images. The longer the image data stays on the CCD the more this value increases.
6. Response differences among different CCD cameras.
7. Different capturing angle and illumination conditions caused by the tilted focal planes.

To form a large-format PAN virtual image, each of the involved camera heads are first radiometrically calibrated on the basis of camera calibration data. However, radiometric differences between adjacent PAN images may remain; therefore, the platform radiometric calibration is needed. A histogram of the pixels in the overlapping regions of the images is derived to correct the remaining radiometric differences. Then, an optimization of the intensity values is computed and applied during the mosaicking process (Diener *et al.* 2000; Heier *et al.*, 2002). But each overlapping region of the images is very small, and the derived histogram information from local regions may not reflect the radiometric differences of the entire PAN images. To this end, the platform calibration will fail to remove the radiometric differences. And, if the radiometric differences are corrected in a relatively narrow area, there will be residual radiometric differences in the final color composite DMC images.

Let I_1 and I_2 be the left and right CCD image, respectively; W be the weight function, and $\Delta g(x, y)$ be the radiometric differences between CCD images around the transition area. Let R_L, R_T and R_R be the left image area, the transition area and the right image area, respectively. Then, the mosaicking process in radiometry can be denoted as (Burt and Adelson, 1983; Hsu and Wu, 1996):

$$I = \begin{cases} I_1(x, y) & (x, y) \in R_L \\ I_1(x, y) + W(x, y) \cdot \Delta g(x, y) & (x, y) \in R_T \\ I_2(x, y) & (x, y) \in R_R \end{cases}. \quad (1)$$

In Equation 1, $0 \leq W(x, y) \leq 1$, and I is the mosaic result. The proposed algorithm is based on the following idea to remove the residual radiometric differences. If the transition area and seamline are located and the radiometric

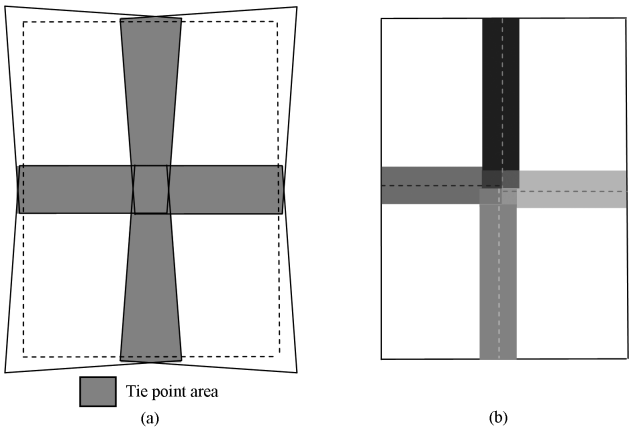

Figure 1. Mosaic procedure of DMC images: (a) the geometric aspect, and (b) the mosaicking procedure.

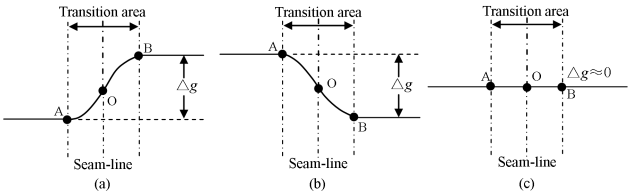

Figure 2. Section map across transition area: (a) and (b) the two cases with radiometric differences, and (c) the case without radiometric differences.

differences $\Delta g(x, y)$ are obtained, the color composite DMC image can be reconstructed, a transition with a wider area can be carried out, and the residual radiometric differences can be removed. In order to achieve such aims, the key step is to locate the transition area and seamline automatically because the positions of the transition area and seamline are (a) not stored in the final DMC images and are varied with different images, (b) needed to calculate the radiometric differences, and (c) required to correct the radiometric differences.

However, there is no considerable discontinuity in color composite DMC images and the radiometric differences occur in a relatively wide area. Therefore, the transition area and seamline can not be located directly. Thus, an indirect method is needed. As shown in Figure 2, the distribution curve is a central symmetry curve and the position of seamline is the center of symmetry in the transition area. Then, point O, the exact position of seamline, is just the midpoint of A and B. So, if getting the position of the transition area, its central point is just the position of seamline.

Feasibility of Locating Transition Area

According to the shape of the distribution curve across the transition area shown in Figure 2, an edge detection operator is used to locate the transition area. An ideal edge is a discontinuity (i.e., a ramp with an infinite slope). The edge detection operator searches the maximum or minimum in the first derivative of the image or zero crossings in the second derivative of the image to find edges. However, changes of pixel values across the transition area take place in a wide area and no discontinuity exists. Therefore, the locating cannot be implemented directly by an edge detection operator.

Due to the stability of pixel values in CCD images and different CCD images for mosaicking have been calibrated, I_1 and I_2 can be ideally viewed as two planes with different "height." Therefore, in one dimension, let $I_1(x) = a_1$ and $I_2(x) = a_2$, and then $\Delta g = a_2 - a_1 \neq 0$. Let the coordinates of points A and B are x_A and x_B, respectively, and then Equation 1 becomes:

$$I = \begin{cases} a_1 & x < x_A \\ a_1 + W(x) \cdot (a_2 - a_1) & x_A \leq x \leq x_B. \\ a_2 & x_B < x \end{cases} \quad (2)$$

According to Meunier and Borgmann (2000), polynomial weighting is used to model the radiometric transition:

$$W(x) = \frac{(x - x_A)^n}{(x - x_A)^n + (x_B - x)^n}. \quad (3)$$

Let $w = x_B - x_A$ and $u = (x - x_A)/w$, Equation 3 can be simplified as:

$$W(u) = \frac{u^n}{u^n + (1 - u)^n}. \quad (4)$$

When $n = 1$, $W(u) = u$. Then, the weight function W becomes a linear function, and it is consistent with the simplest weight function in mosaic processing (Milgram 1975; Zhu and Qian 2002). As $W(x) = 0$ for $x = x_A$ and $W(x) = 1$ for $x = x_B$, I is differentiable, and its derivative can be denoted as:

$$\frac{\partial I}{\partial u} = \begin{cases} 0 & u < 0 \\ a_2 - a_1 & 0 \leq u \leq 1. \\ 0 & 1 < u \end{cases} \quad (5)$$

Then, at points A and B, $\frac{\partial I}{\partial u}$ is not differentiable and some discontinuities exist. The positions of points A and B can be detected by an edge detection operator.

When $n = 2$, $W(u) = \dfrac{u^2}{u^2 + (1 - u)^2}$. The first derivative of I is:

$$\frac{\partial I}{\partial u} = \begin{cases} 0 & u < 0 \\ (a_2 - a_1)(-2u^2 + 2u)/(2u^2 - 2u + 1)^2 & 0 \leq u \leq 1. \\ 0 & 1 < u \end{cases} \quad (6)$$

The second derivative of I is:

$$\frac{\partial^2 I}{\partial u} = \begin{cases} 0 \\ (a_2 - a_1)(8u^3 - 12u^2 + 2)/(2u^2 - 2u + 1)^3 \\ 0 \end{cases} \quad \begin{matrix} u < 0 \\ 0 \leq u \leq 1. \\ 1 < u \end{matrix} \quad (7)$$

Then, at points A and B, $\frac{\partial^2 I}{\partial u}$ is not differentiable, and some discontinuities exist. The positions of points A and B can be detected by an edge detection operator.

In a similar way, when $n = 3$ at points A and B, $\frac{\partial^3 I}{\partial u}$ is not differentiable and some discontinuities exist. And when $n = 4$ at points A and B, $\frac{\partial^4 I}{\partial u}$ is also not differentiable and some discontinuities exist. For higher n, the similar conclusion can be drawn. Generally, the value for n is between 3 and 4. The larger parameter n is, the sharper the transition between the images, and the less blurred the transition area appears (Meunier and Borgmann, 2000).

In summary, whatever the parameter n of the weight function is, the n^{th} derivative of I is not differentiable at points A and B. In other words, there are always discontinuities at points A and B in n^{th} derivative, thus the positions of A and B can be detected. The area between points A and B is just the transition area and the midpoint between A and B is the position of seamline. The proof for locating the transition area is illustrated in Figure 3 for two cases: when $n = 1$ and $n = 2$, are illustrated, respectively.

The above proof is based on a continuous distribution, but the image is in discrete format, and the distribution curve is observed in the discrete case. Therefore, the derivative is replaced by the difference. In practice it appears that using $n = 1$ to approximate the weight function suffices to generally produce practical results.

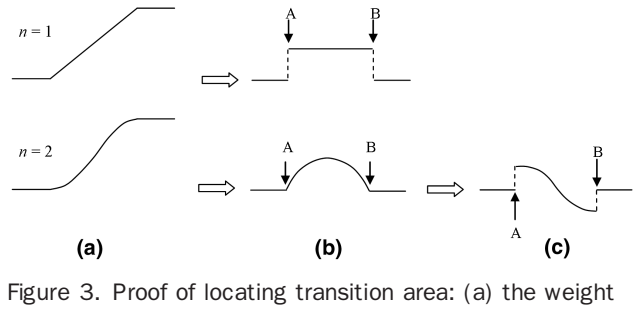

Figure 3. Proof of locating transition area: (a) the weight function, (b) the first derivative, and (c) the second derivative.

Methods

Our proposed approach comprises the auto-locating for the transition area and seamline and the subsequent reconstruction for image in radiometry. There are four transition areas in one individual color composite DMC image. The auto-locating for the transition area and seamline and the subsequent reconstruction for image in radiometry are performed in each transition area respectively.

Autolocating Based on Hierarchical Strategy

As shown in Figure 2, three possible cases may occur in different parts of the same transition area, which makes auto-locating difficult. Nevertheless, in one part of the transition area, only one case would occur and then auto-locating will be easier. Under such recognition, the transition area is divided into small blocks, and positions of the transition area and seamline are detected in each block, respectively.

On the other hand, by analyzing color composite DMC images, the seamline between CCD images is a straight line, either vertical or horizontal, and the change of features may destroy the local similarity in the transition area and affect the distribution curve of pixel values across the transition area. Therefore, the mean of each row or column parallel to the seamline is taken in order to obtain stable distribution curve in one-dimension (1D). Also, the use of a 1D smoothing filter to the initial distribution curve is beneficial to get stable distribution curve.

In this paper, an edge-detection operator is adopted to locate the transition area. However, current edge-detection methods can be applied only to a single-band image (Wang *et al.*, 2004). Therefore, the luminance channel image is calculated and selected as the single-band image for auto-locating, given the fact that the residual radiometric differences are mainly caused by the formation of the large format PAN virtual image.

The auto-locating process is performed hierarchically for the robustness. There are six main steps:

1. The middle part between two adjacent CCD images is considered as the search area. The luminance channel image is calculated and selected as the single-band image for locating.
2. The luminance channel image of the search area is divided into blocks. Generally, one search area is divided into ten blocks. Each block contains a part of seamline (see Figure 4). The middle area denotes the search area and dashed line denotes the seamline.
3. An image pyramid of the luminance channel image is calculated. A reduction factor of 3 is used with a 3×3 Gaussian filter. Pyramid calculation is terminated when the width of the luminance channel image is less than 25 pixels.
4. The mean of each row or column parallel to the seamline is taken to form the initial distribution curve for each block of each pyramid level. Then, a 1D mean filter with a size of 3 is used to the initial distribution curve. The second difference of distribution curve is also calculated.
5. The detection of the transition area for each block from the second difference and the middle position of the transition area is considered as the position of the seamline. The detection process is carried out from top to bottom pyramid levels. As to the top pyramid level, the maximum and minimum values in the second difference are located, and their positions delineate the transition area. As to the following pyramid level, the positions searched from the previous pyramid level will be considered as the initial positions. More accurate positions are searched in a relatively narrow range around the initial positions. The process of detecting the transition area for a block is illustrated in Figure 5. The search rules for the transition area refinement are as follows.

   Let M_L and M_R denote the means calculated by areas with a certain size on the left and right side of the transition area, respectively, and let δ denote the threshold for radiometric difference to judge which case in Figure 2 it belongs:

   - Figure 2a depicts the case when $(M_L - M_R) < -\delta$. From the second difference of distribution curve, the maximum value around the initial start position of the transition area and the minimum value around the initial end position of the transition area are searched. And these positions are the positions of the transition area at the current pyramid level.
   - Figure 2b shows the case when $(M_L - M_R) > \delta$. The minimum value around the initial start position and the maximum value around the initial end position are searched.
   - Figure 2c depicts the case when $|M_L - M_R| < \delta$. This block is ignored.
6. A voting strategy is used to obtain the final positions of the transition area. Positions detected from each block are counted and the positions with the highest frequency are considered as the final positions of the transition area. The middle position of the transition area is considered as the position of the seamline.

Reconstruction in Radiometry

A multi-scale strategy with two different spatial scales is used to optimize the subsequent reconstruction in radiometry, in which two main steps are conducted: (a) "break" processing, and (b) "seam" removal.

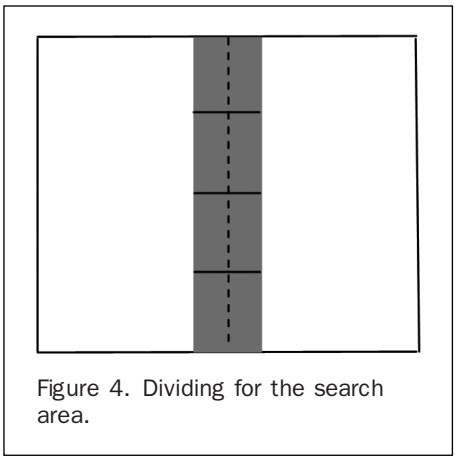

Figure 4. Dividing for the search area.

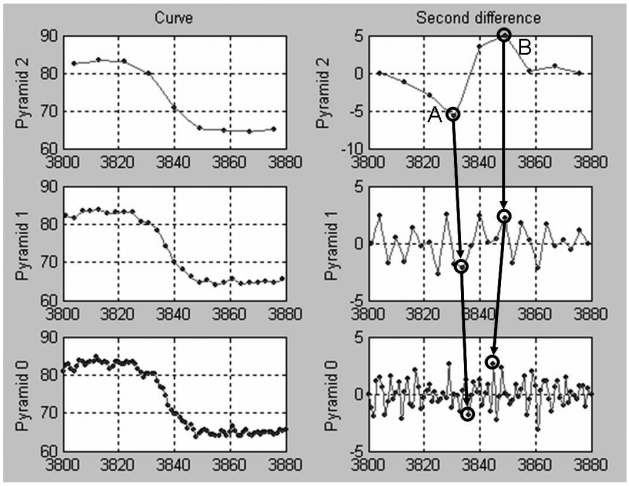

Figure 5. Process of detecting the transition area.

The "break" processing is carried out in a large scale. It removes the radiometric differences between CCD images in a wide area out of the transition area and breaks the continuity of original pixel values around the seamline. The "seam" removal is carried out in a small scale, and it removes the new "seam" formed by the "break" processing.

"Break" Processing

The "break" processing step reconstructs the image around the transition area based on the seamline. In a wide area at both sides of the transition area, it removes the radiometric differences between CCD images. In the transition area, it breaks the continuity of pixel values. The break processing is detailed as follows:

1. Divide the seamline into small parts.
2. Calculate the radiometric differences for each part of the seamline. The radiometric differences between CCD images are the main factor causing the residual radiometric differences. As shown in Figure 2, the differences of means calculated by areas with a width of 20 pixels at both sides of the transition area are taken as the initial radiometric differences between the CCD images. Because the change of features may affect the calculated radiometric differences between CCD images, a 1D mean filter is used to the initial radiometric differences.
3. Remove the radiometric differences for each part of the seamline by linearization. This operation is conducted in a wider area in order to achieve a more smooth transition. The correction value varies as a function of the distance from the seamline. The pixels closer to the seamline will have bigger correction value and at the position of the seamline, the correction value is half of the radiometric differences. This is similar to the seamline removal algorithm in mosaicking (Milgram, 1975; Zhu and Qian, 2002).

The "break" processing in 1D is illustrated in Figure 6. The dashed lines denote the original distribution of pixel values, and solid lines denote the distribution after "break" processing. The processing is carried out on each side of seamline in an area with width L, respectively. Because the original distribution of pixel values is continuous, the "break" processing will form a new "seam" at the position of seamline.

"Seam" Removal

The "seam" removal step removes the new visible "seam" by linearization. It is carried out in the transition area. The key problem for "seam" removal is to obtain the proper correction values.

Let $\Delta g'$ denote the radiometric differences between points A and B (the area between points A and B is the transition area) and let $f(x)$ denote the distribution curve after "break" processing. At point A, let $f(x_A) = y_A$; and at point B, let $f(x_B) = y_B$. Then in 1D, the expectation image across the transition area is a straight line with slope $\Delta g'/(x_B - x_A)$. Because the point A is on the line, in 1D the expectation image I_E can be denoted as:

$$I_E = \frac{(x - x_A)\Delta g'}{x_B - x_A.} + y_A. \tag{8}$$

Let I_B denotes the image after "break" processing, then the correction value will be $I_E - I_B$. To this end, the proper correction value can be calculated easily.

The "seam" removal is detailed as follows:

1. Divide the seamline into small parts. Compared with the "break" processing, the size of each part of the seamline is smaller.
2. Calculate the initial radiometric differences for each part of the seamline. This is similar to that in the "break" processing except for the width of areas at both sides of the transition area. A width of three pixels is sufficient. The final radiometric difference for each small part of the seamline is interpolated by the initial radiometric differences of the nearest two small parts of the seamline.
3. Use Equation 8 to calculate the correction value for each pixel and update the value of each pixel.

The "seam" removal in 1D is illustrated in Figure 7. The dashed lines denote the result after "break" processing, and there is a jump in pixel values around the seamline. The solid line denotes the result after "seam" removal, and clearly there is a more smooth transition.

Experimental Results

A number of images with residual radiometric differences were employed to test the proposed algorithm. The test images were produced from a postprocessed DMC image with dimensions of 7,680 pixels by 13,824 pixels. Figure 8 shows this color composite DMC image with residual radiometric differences and six detailed regions. It can be seen that the transition area between CCD images is not smooth enough in radiometry and the same feature appears in different colors. Figure 8b shows the derived image ob-tained by the proposed algorithm and Figure 8i through 8n are the corresponding areas of Figure 8c through 8h in derived image, respectively. The auto-locating is implemented in the luminance channel. The middle area between two adjacent CCD images with a width of 297 pixels is considered as the search area and four pyramids are calculated. The subsequent reconstruction is carried out in each channel of RGB,

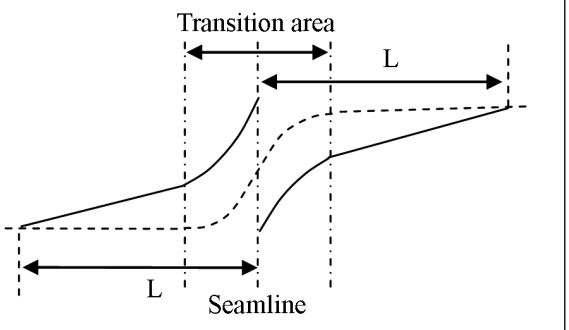

Figure 6. "Break" processing.

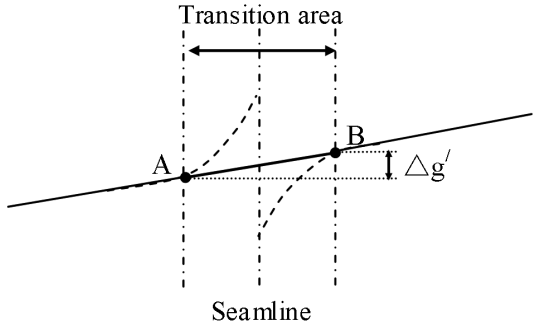

Figure 7. "Seam" removal.

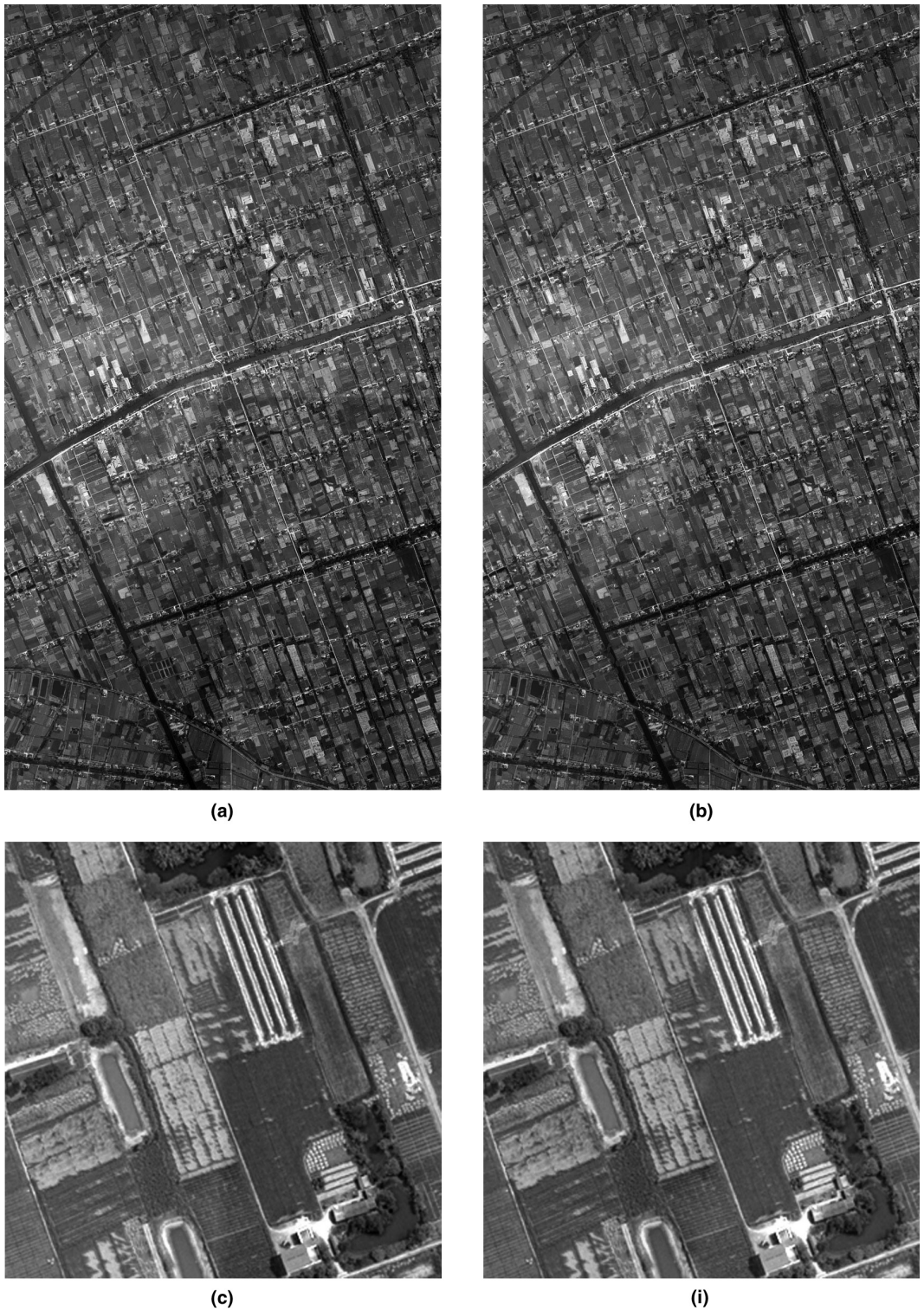

Figure 8. (a) Original color composite DMC image, (b) derived image, (c) through (h) detailed regions of original image, and (i) through (n) corresponding areas in the revised image, respectively. A color version of this figure is available at the ASPRS website: **www.asprs.org**.

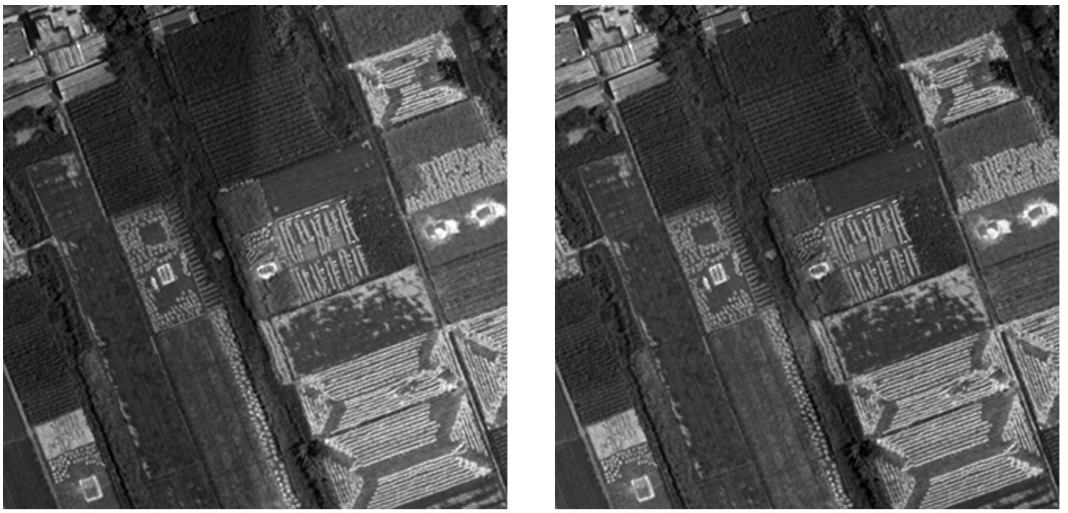

(d) (j)

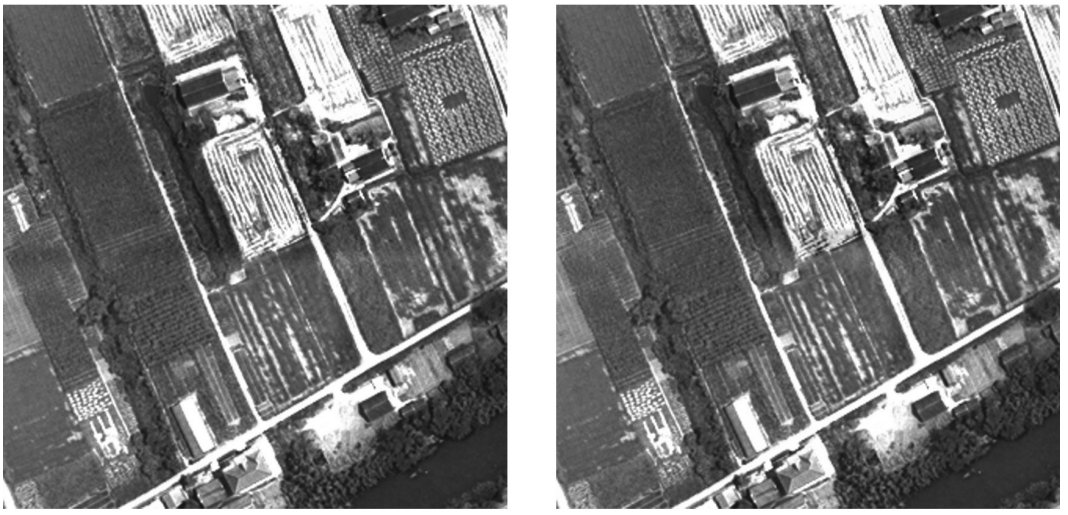

(e) (k)

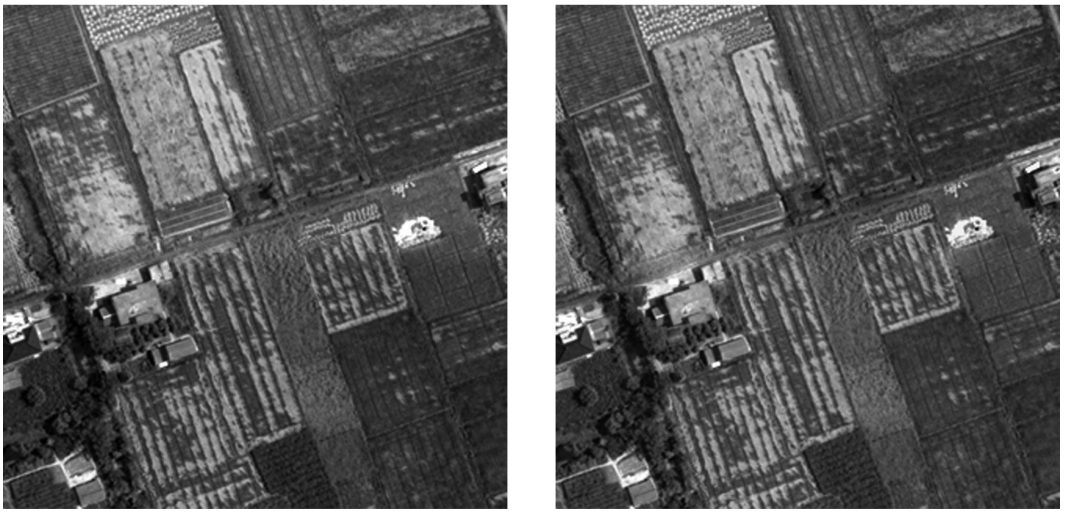

(f) (l)

Figure 8. (Continued) (a) Original color composite DMC image, (b) derived image, (c) through (h) detailed regions of original image, and (i) through (n) corresponding areas in the revised image, respectively. A color version of this figure is available at the ASPRS website: **www.asprs.org**.

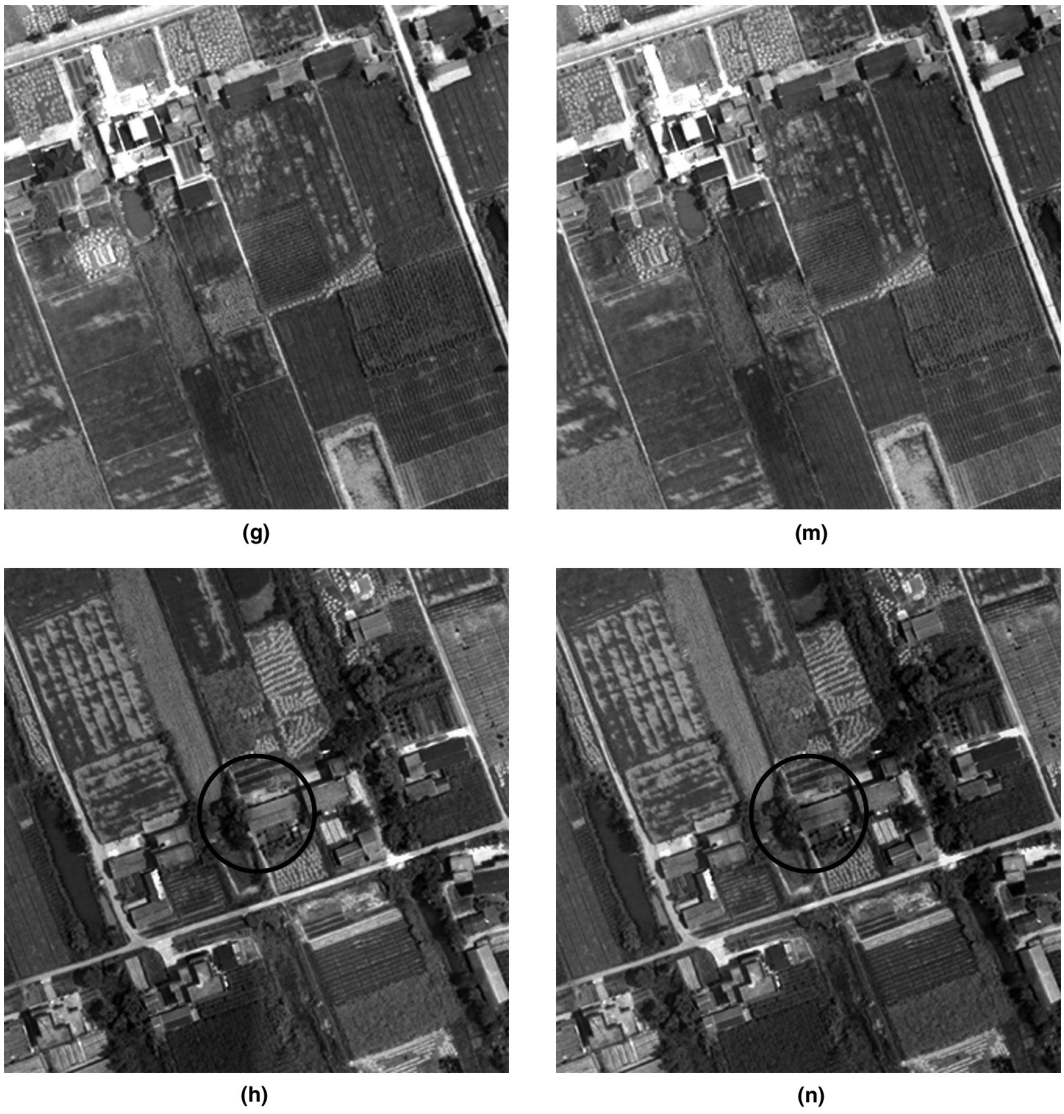

Figure 8. (Continued) (a) Original color composite DMC image, (b) derived image, (c) through (h) detailed regions of original image, and (i) through (n) corresponding areas in the revised image, respectively. A color version of this figure is available at the ASPRS website: **www.asprs.org**.

respectively. The "break" processing is carried out on each side of seamline in an area with a width of 500 pixels, respectively. In the "break" processing, the seamline is divided into small parts with a size of 100 pixels and the size of the 1D mean filter is 5. In the "seam" removal, the seamline is divided into small parts with a size of 30 pixels.

In order to evaluate the performance of the proposed approach, both qualitative (visual inspection) and quantitative (statistical analysis) evaluations are conducted. Visually comparing with original image shown in Figure 8a and processed image shown in Figure 8b suggests that most residual radiometric differences have been successfully removed. It also should be noticed that the proposed radiometric adjustment may distort the given DMC image negatively. Figure 8h and 8n show an example and the distorted area marked by circle. It can be seen that the grayscale of the roof was distorted after processing. In a quantitative aspect, the grayscale differences before and after processing of the same features are chosen to provide statistical values. As summarized in Table 1, a total of 40 sample pairs around the transition area were chosen. Each sample pair represents one type of land-cover and land-use features (e.g., house, tree, grass, bare ground, water, farmland, and road). The grayscale differences of each sample pair are calculated by the mean differences of the sample pair in each channel. The mean is calculated by the adjacent area of the sample point with a size of 5 pixels by 5 pixels. From Table 1, the grayscale differences of most sample pairs are decreased to a small value. Three sample pairs are highlighted in Table 1, as their pixel values are distorted. In summary, experiments achieve a success and indicate that the proposed algorithm is feasible and effective. But, it should still be optimized because the algorithm may distort the given DMC image negatively.

Conclusions

The color composite image repairing approach proposed in this paper appears to effectively detect and remove the

TABLE 1. GRAYSCALE DIFFERENCES BEFORE AND AFTER PROCESSING

	Original Image			Derived Image		
Sample Pairs	Red	Green	Blue	Red	Green	Blue
1	−21.60	−27.16	−43.64	2.36	1.20	−5.04
2	−20.56	−27.52	−28.88	−0.24	−1.44	4.48
3	−29.36	−39.72	−45.64	−4.52	−8.56	−1.48
4	−25.24	−35.28	−45.96	−5.24	−7.28	−6.36
5	−28.72	−33.56	−47.48	−7.00	−4.48	−6.60
6	−25.88	−31.96	−37.96	0.80	2.12	6.48
7	−31.52	−39.20	−48.08	−8.52	−7.20	−8.16
8	25.24	34.08	47.04	−2.28	−2.88	1.60
9	−28.24	−36.16	−50.56	−5.24	−3.16	−10.56
10	−8.20	−16.08	−35.56	0.80	4.00	−2.56
11	−28.56	−29.32	−30.44	−4.40	2.56	9.20
12	−37.24	−43.60	−54.72	6.08	6.16	−5.72
13	−8.96	−17.24	−24.96	−14.72	−5.72	−0.68
14	−21.36	−26.60	−35.60	−5.84	−4.24	−6.44
15	−19.88	−25.80	−33.92	−0.60	0.56	−1.00
16	−21.24	−29.00	−31.60	−1.44	−2.24	−0.08
17	10.60	17.04	15.56	16.04	11.12	1.00
18	−21.08	−21.44	−31.16	−3.20	3.80	0.52
19	−18.32	−17.56	−28.44	−2.64	2.48	−1.04
20	13.80	19.72	22.56	−7.36	−2.44	−4.32
21	−20.36	−30.12	−36.36	9.72	−1.48	1.32
22	−28.12	−27.16	−31.56	−6.52	−1.52	−1.56
23	−11.56	−22.20	−34.36	8.44	2.80	−5.36
24	29.52	14.20	13.84	35.36	13.00	4.96
25	14.36	19.20	30.00	2.28	−2.80	4.00
26	6.04	11.52	11.84	3.76	5.92	4.88
27	22.72	23.64	38.20	−7.92	−3.08	8.56
28	15.08	23.20	27.48	−4.16	2.36	0.96
29	20.60	21.96	26.20	6.36	2.00	−1.20
30	10.00	16.96	19.64	−2.68	−1.88	−3.92
31	16.64	22.40	23.76	2.40	3.24	−1.12
32	13.84	18.88	19.12	−0.16	1.44	−1.40
33	7.72	10.40	18.36	−4.80	−5.96	−4.76
34	13.04	16.48	23.48	−3.56	−4.96	−6.08
35	24.48	20.32	27.96	8.84	1.36	2.16
36	11.96	15.40	23.36	2.12	1.88	2.80
37	15.04	23.68	26.96	1.40	3.60	−0.16
38	16.28	20.48	32.24	0.20	−1.64	2.08
39	16.56	22.72	28.44	−5.44	−5.32	−7.12
40	19.60	21.76	28.88	0.44	−0.52	−3.20

residual radiometric differences between CCD images acquired by the DMC. The approach consists of two main steps: the auto-locating of the transition area and seamline, and the subsequent reconstruction based on the seamline in radiometry. The complexity of the distribution of pixel values makes the auto-locating and the subsequent reconstruction more difficult. In order to overcome such difficulty, a differential idea was adopted by dividing the processing area into small sub-areas to simplify the problem, and a hierarchical strategy was used. Another difficulty is that the change of features may destroy the similarity of local area, which will affect the distribution curve of pixel values and the radiometric differences between CCD images. The small sub-areas were considered as computing cells, and a smooth filter was used in a multi-scale strategy to overcome this difficulty. Given the fact that existing edge detection methods only work well on a single-band image and the residual radiometric differences are mainly caused by the formation of the large format PAN virtual image, the auto-locating process was carried out in the luminance channel. The subsequent reconstruction was carried out in each channel of RGB, respectively, because the fusion of high-resolution PAN image and low-resolution RGB image finally changed the luminance, hue, and saturation simultaneously, and reconstruction only in the luminance channel could not remove the residual radiometric differences effectively. The proposed approach is a relative radiometric calibration in a sense, and its aim is to remove the radiometric differences of the same features between CCD images. Both qualitative and quantitative analyses were applied to evaluate the performance. Our experiments illustrated that the quality of the color composite DMC images with residual radiometric differences can be considerably improved by the proposed algorithm. Moreover, our algorithm demonstrated more robust in successfully repairing the color composite DMC images with residual radiometric differences compared with other previous work. The algorithm has been embedded into GeoDodging 4.0 software package as a complementary module for the postprocessing of DMC images.

The primary drawback of the proposed algorithm in its present form is that it may distort the given DMC image negatively. The reason is that the proposed approach is based on the assumption that features in local area have great similarity in radiometry. In most cases, such an assumption is met and some strategies have been adopted to reinforce the robustness of the proposed approach. When the assumption is not met, using more robust strategies to optimize the adjustment may avoid the distortion and further improve the

results. Optimization in the gradient domain (Levin *et al.* 2004; Zomet *et al.* 2006) may also improve the results. From a user's point of view, a tool which can directly repair the color composite DMC image would be more helpful. The algorithm for adjusting the PAN virtual image directly, and being embedded into the post-processing of DMC images is also a further developing direction.

Acknowledgments

The research described in this paper was funded by National Key Basic Research and Development Program of China (No. 2006CB701302) and the Youth Foundation Plan of Wuhan, China (No. 200750731253). Images for experiments were provided by Wuda Geoinformatics Co., Ltd.

References

Afek, Y., and A. Brand, 1998. Mosaicing of orthorectified aerial image, *Photogrammetric Engineering & Remote Sensing*, 64(2):115–125.

Burt, P.J., and E.H. Adelson, 1983. A multiresolution spline with application to image mosaics, *ACM Transactions on Graphics*, 2(4):217–236.

Diener, S., M. Kiefner, and C. Dörstel, 2000. Radiometric normalisation and colour composite generation of the DMC, *International Archives of Photogrammetry and Remote Sensing*, 13–16 July, Amsterdam, Vol. 33, Part B1, pp. 82–88.

Dörstel, C., and W. Zeitler, 2002. Geometric calibration of the DMC: Method and results, *International Archives for Photogrammetry and Remote Sensing*, 34(1):324–333.

DiMAC Systems, 2007, URL: *http://www.dimac-camera.com/* (last date accessed: 12 November 2008).

Hsu C.T., and J.L. Wu, 1996. Multiresolution mosaic, *IEEE Transactions on Consumer Electronics*, 42(4):981–990.

Hinz, A., C. Dörstel, and H. Heier, 2000. Digital Modular Camera: System concept and data processing workflow, *International Archives of Photogrammetry and Remote Sensing*, 13–16 July, Amsterdam, Vol. 33, Part B2, pp.164–171.

Heier, H., M. Kiefner, and W. Zeitler, 2002. Calibration of the digital modular camera DMC, *Proceedings of the 22nd FIG International Congress*, 19–26 April, Washington, D.C., unpaginated CD-ROM.

Levin A., A. Zomet, S. Peleg, and Y. Weiss, 2004. Seamless image stitching in the gradient domain, *Proceedings of the 8th European Conference on Computer Vision*, 11–14 May, Prague, pp. 377–389.

Milgram, D.L., 1975. Computer methods for creating photomosaics, *IEEE Transactions on Computers*, C-24(11):1113–1119.

Madani M., C. Dörstel, C. Heipke, and K. Jacobsen, 2004. DMC practical experience and accuracy assessment, 12–23 July, Istanbul, *International Archives of the Photogrammetry, Remote Sensing and Spatial Information Sciences*, Vol. 34, B2, pp. 396–401.

Meunier, L., and M. Borgmann, 2000, High-resolution panoramas using image mosaicing, URL: *http://scien.stanford.edu/class/ee368/projects2000/project13/index.html*, EE368 Project, Spring, Stanford University (last date accessed: 12 November 2008).

Pan J., M. Wang, and D.R. Li, 2006. Self-adaptive repair approach for color composite DMC images, *Proceedings of the 14th International Conference on Geoinformatics*, 28–29 October, Wuhan, China, unpaginated CD-ROM.

Tang, L., C. Dörstel, K. Jacobsen, C. Heipke, and A. Hinz, 2000. Geometric accuracy potential of the digital modular cameral, *International Archives of the Photogrammetry, Remote Sensing and Spatial Information Sciences*, 13–16 July, Amsterdam, Vol. 33, Part B4/3, pp. 1051–1057.

Vexcel, 2008, URL: *http://www.vexcel.com/* (last date accessed: 12 November 2008).

Wang, L., P. Gong, and G.S. Biging, 2004. Individual tree-crown delineation and treetop detection in high-spatial-resolution aerial imagery, *Photogrammetric Engineering & Remote Sensing*, 70(3):351–357.

Wang, M., J. Pan and T.T. Feng, 2005. A radiometric post-processing approach to color composite DMC images, *Proceedings of the 4th International Symposium on Multispectral Image Processing and Pattern Recognition*, 31 October-02 November, Wuhan, China, unpaginated CD-ROM.

Zhu, S.L., and Z.B. Qian, 2002. The seamline removal under mosaicking of remotely sensed images, *Journal of Remote Sensing*, 3(3):183–187.

Zomet A., A. Levin, S. Peleg, and Y. Weiss, 2006. Seamless image stitching by minimizing false edges, *IEEE Transactions on Image Processing*, 15(4):969–977.

(Received 27 July 2007; accepted 09 November 2007; revised 14 December 2007)